

Fully 3D Multiple Beam Dynamics Processes Simulation for the Tevatron

E.G. Stern,* J.F. Amundson, P.G. Spentzouris, and A.A. Valishev

Fermi National Accelerator Laboratory

(Dated: August 6, 2009)

Abstract

We present validation and results from a simulation of the Fermilab Tevatron including multiple beam dynamics effects. The essential features of the simulation include a fully 3D strong-strong beam-beam particle-in-cell Poisson solver, interactions among multiple bunches and both head-on and long-range beam-beam collisions, coupled linear optics and helical trajectory consistent with beam orbit measurements, chromaticity and resistive wall impedance. We validate individual physical processes against measured data where possible, and analytic calculations elsewhere. Finally, we present simulations of the effects of increasing beam intensity with single and multiple bunches, and study the combined effect of long-range beam-beam interactions and transverse impedance.

PACS numbers: 29.27.-a

*Electronic address: egstern@fnal.gov

I. MOTIVATION

The Fermilab Tevatron [1] is a $p\text{-}\bar{p}$ collider operating at a center-of-mass energy of 1.96 TeV and peak luminosity reaching $3.53 \times 10^{32} \text{ cm}^{-2} \text{ s}^{-1}$. The colliding beams consist of 36 bunches moving in a common vacuum pipe. For high-energy physics operations, the beams collide head-on at two interaction points (IPs) occupied by particle detectors. In the arcs the beams are separated by means of electrostatic separators and long-range (also referred to as parasitic) collisions occur at 136 other locations. Effects arising from both head-on and long-range beam-beam interactions impose serious limitations on machine performance, hence constant efforts are being exerted to better understand the beam dynamics. Due to extreme complexity of the problem a numerical simulation appears to be one of the most reliable ways to study performance of the system.

Studies of beam-beam interactions in the Tevatron Run II mainly concentrated on the incoherent effects, which were the major source of particle losses and emittance growth. This approach was justified by the fact that the available antiproton intensity was a factor of 10 to 5 less than the proton intensity with approximately equal transverse emittances. Several simulation codes were developed and used for optimization of the collider performance [2], [3].

With the commissioning of electron cooling in the Recycler, the number of antiprotons available to the collider substantially increased. During the 2007 and 2008 runs the initial proton and antiproton intensities differed by only a factor of 3. Moreover, the electron cooling produces much smaller transverse emittance of the antiproton beam ($\simeq 4 \pi \text{ mm}\cdot\text{mrad}$ 95% normalized vs. $\simeq 20 \pi \text{ mm}\cdot\text{mrad}$ for protons), leading to the head-on beam-beam tune shifts of the two beams being essentially equal. The maximum attained total beam-beam parameter for protons and antiprotons is 0.028.

Under these circumstances coherent beam-beam effects may become an issue. A number of theoretical works exist predicting the loss of stability of coherent dipole oscillations when the ratio of beam-beam parameters is greater than $\simeq 0.6$ due to the suppression of Landau damping [4]. Also, the combined effect of the machine impedance and beam-beam interactions in extended length bunches couples longitudinal motion to transverse degrees of freedom and may produce a dipole or quadrupole mode instability [5].

Understanding the interplay between all these effects requires a comprehensive simulation.

This paper presents a macroparticle simulation that includes the main features essential for studying the coherent motion of bunches in a collider: a self-consistent 3D Poisson solver for beam-beam force computation, multiple bunch tracking with the complete account of sequence and location of long-range and head-on collision points, and a machine model including our measurement based understanding of the coupled linear optics, chromaticity, and impedance.

In Sections II–V we describe the simulation subcomponents and their validation against observed effects and analytic calculations. Section VI shows results from simulation runs which present studies of increasing the beam intensity. Finally, in Section VII we study the coherent stability limits for the case of combined resistive wall impedance and long-range beam-beam interactions.

II. BEAMBEAM3D CODE

The Poisson solver in the BeamBeam3d code is described in Reference [6]. Two beams are simulated with macro-particles generated with a random distribution in phase space. The accelerator ring is conceptually divided into arcs with potential interaction points at the ends of the arcs. The optics of each arc is modeled with a 6×6 linear map that transforms the phase space $\{x, x', y, y', z, \delta\}$ coordinates of each macroparticle from one end of the arc to the other. There is significant coupling between the horizontal and vertical transverse coordinates in the Tevatron. For our Tevatron simulations, the maps were calculated using coupled lattice functions [7] obtained by fitting a model [8] of beam element configuration to beam position measurements. The synchrotron motion is put in as a sinusoidal oscillation with the periodicity of the machine synchrotron tune. Chromaticity results in an additional momentum dependent phase advance $\delta\mu_{x(y)} = \mu_0 C_{x(y)} \Delta p/p$ where $C_{x(y)}$ is the chromaticity for x (or y) and μ_0 is the design phase advance for the arc. The additional phase advance is applied to each particle in the decoupled coordinate basis so that symplecticity is preserved.

The Tevatron includes electrostatic separators to generate a helical trajectory for the oppositely charged beams. The mean beam offset at the IP is included on the Poisson field solver calculation.

Different particle bunches are individually tracked through the accelerator. They interact with each other with the pattern and locations that they would have in the actual collider.

The impedance model applies a momentum kick to the particles generated by the dipole component of resistive wall wakefields [10]. Each beam bunch is divided longitudinally into slices containing approximately equal numbers of particles. As each bunch is transported through an arc, particles in slice i receive a transverse kick from the wake field induced by the dipole moment of the particles in forward slice j :

$$\frac{\Delta \vec{p}_\perp}{p} = \frac{2}{\pi b^3} \sqrt{\frac{4\pi\epsilon_0 c}{\sigma}} \frac{N_j r_p \langle \vec{r}_j \rangle}{\beta\gamma} \frac{L}{\sqrt{z_{ij}}} \quad (1)$$

The length of the arc is L , N_j is the number of particles in slice j , r_p is the classical electromagnetic radius $e^2/4\pi\epsilon_0 mc^2$, z_{ij} is the longitudinal distance between the particle in slice i that suffers the wakefield kick and slice j that induces the wake. \vec{r}_j is the mean transverse position of particles in slice j , b is the pipe radius, c is the speed of light, σ is the conductivity of the beam pipe and $\beta\gamma$ are Lorentz factors of the beam. Quantities with units are specified in the MKSA system.

III. SYNCHRO-BETATRON COMPARISONS

We will assess the validity of the beam-beam calculation by comparing simulated synchro-betatron mode tunes with a measurement performed at the VEPP-2M 500 MeV e^+e^- collider and described in Reference [11]. These modes are an unambiguous marker of beam-beam interactions and provide a sensitive tool for evaluating calculational models. These modes arise in a colliding beam accelerator where the longitudinal bunch length and the transverse beta function are of comparable size. Particles at different z positions within a bunch are coupled through the electromagnetic interaction with the opposing beam leading to development of coherent synchro-betatron modes. The tune shifts for different modes have a characteristic evolution with beam-beam parameter $\xi = Nr_0/4\pi\gamma\epsilon$, in which N is the number of particles, r_0 is the classical electromagnetic radius, and ϵ is the beam emittance.

There are two coherent transverse modes in the case of simple beam-beam collisions between equal intensity beams without synchrotron motion: the σ mode where the two beams oscillate with the same phase, and the π mode where the two beams oscillate with opposite phases [12]. Without synchrotron motion, the σ mode has the same tune as unperturbed betatron motion while the π mode frequency is offset by $K\xi$, where the parameter K is approximately equal to 1 and depends on the transverse shape of the beams

[13]. The presence of synchrotron motion introduces a more complicated spectrum of modes whose spectroscopy is outlined in Fig. 1 in Reference [11]

We simulated the VEPP-2M collider using Courant-Snyder uncoupled maps. The horizontal emittance in the VEPP-2M beam is much larger than the vertical emittance. The bunch length (4 cm) is comparable to $\beta_y^* = 6$ cm so we expect to see synchrobetatron modes. In order to excite synchrobetatron modes, we set an initial y offset of one beam sigma approximately matching the experimental conditions.

Longitudinal effects of the beam-beam interaction were simulated by dividing the bunch into six slices. At the interaction point, bunches drift through each other. Particles in overlapping slices are subjected to a transverse beam-beam kick calculated by solving the 2D Poisson equation for the electric field with the charge density from particles in the overlapping beam slice.

Fig. 1 shows an example spectrum from a simulation with the three mode peaks indicated. In Fig. 2, the BeamBeam3d simulation of synchro-betatron modes as a function of ξ is plotted on top of experimental data from VEPP-2M. As can be seen, there is good agreement between the observation and simulation giving us confidence in the beam-beam calculation.

IV. IMPEDANCE TESTS

Wakefields or equivalently impedance in an accelerator with a conducting vacuum pipe gives rise to well known instabilities. Our aim in this section is to demonstrate that the wakefield model in BeamBeam3d quantitatively reproduced these theoretically and experimentally well understood phenomena. The strong head-tail instability examined by Chao [10] arises in extended length bunches in the presence of wakefields. For any particular accelerator optical and geometric parameters, there is an intensity threshold, above which the beam becomes unstable.

The resistive wall impedance model applies an additional impulse kick in addition to the application of the map derived from beam optics. The tune spectrum is computed from the Fourier transform of the beam bunch positions sampled at the end of each arc. In order for the calculation to be a good approximation of the wakefield effect, the impedance kick should be much smaller than the x' or y' change due to regular beam transport so we divide the ring into multiple arcs. The relative difference in calculated impedance tune shift for

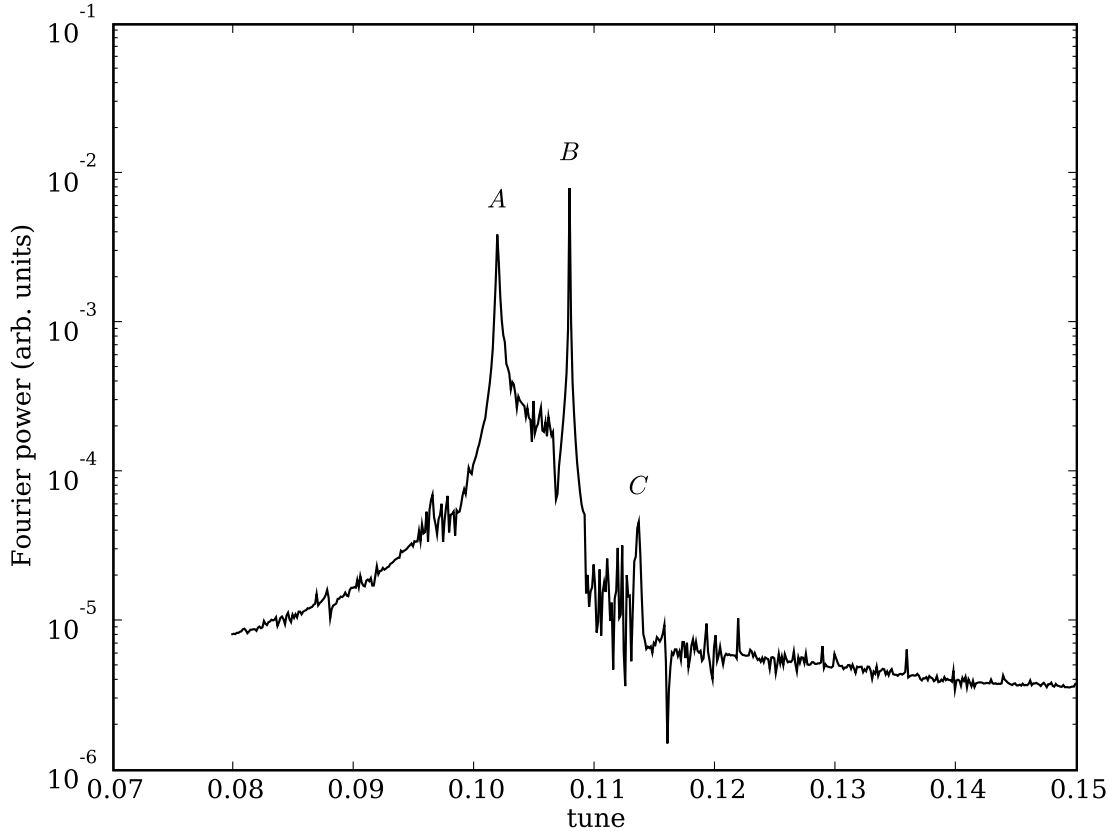


FIG. 1: Simulated mode spectra in the VEPP-2M collider with $\xi = .008$ showing synchro-betatron modes. The line indicated by A is the base tune, B is the first synchro-betatron mode, C is the beam-beam π mode.

a 12 arc division of the ring or 24 arc division results is only 2×10^{-4} so we perform the calculation with 12 arcs for calculational efficiency. In the absence of impedance, we would expect to see the tune spectrum peak at 20.574, the betatron tune of the lattice. With a pipe radius of 3 cm and a bunch length of 20 cm, resistive wall impedance produces the spectrum shown in Fig. 3 for a bunch of 4×10^{12} protons at 150 GeV. The two mode peaks are clearly evident. The upper peak is the betatron frequency shifted down by the wakefield. The lower peak is the lower synchro-betatron mode $20.574 - .007$ shifted upwards by the wakefield.

In Fig. 4, we show the evolution of the two modes as a function of beam intensity. With the tune and beam environment parameters of this simulation, Chao's two particle model

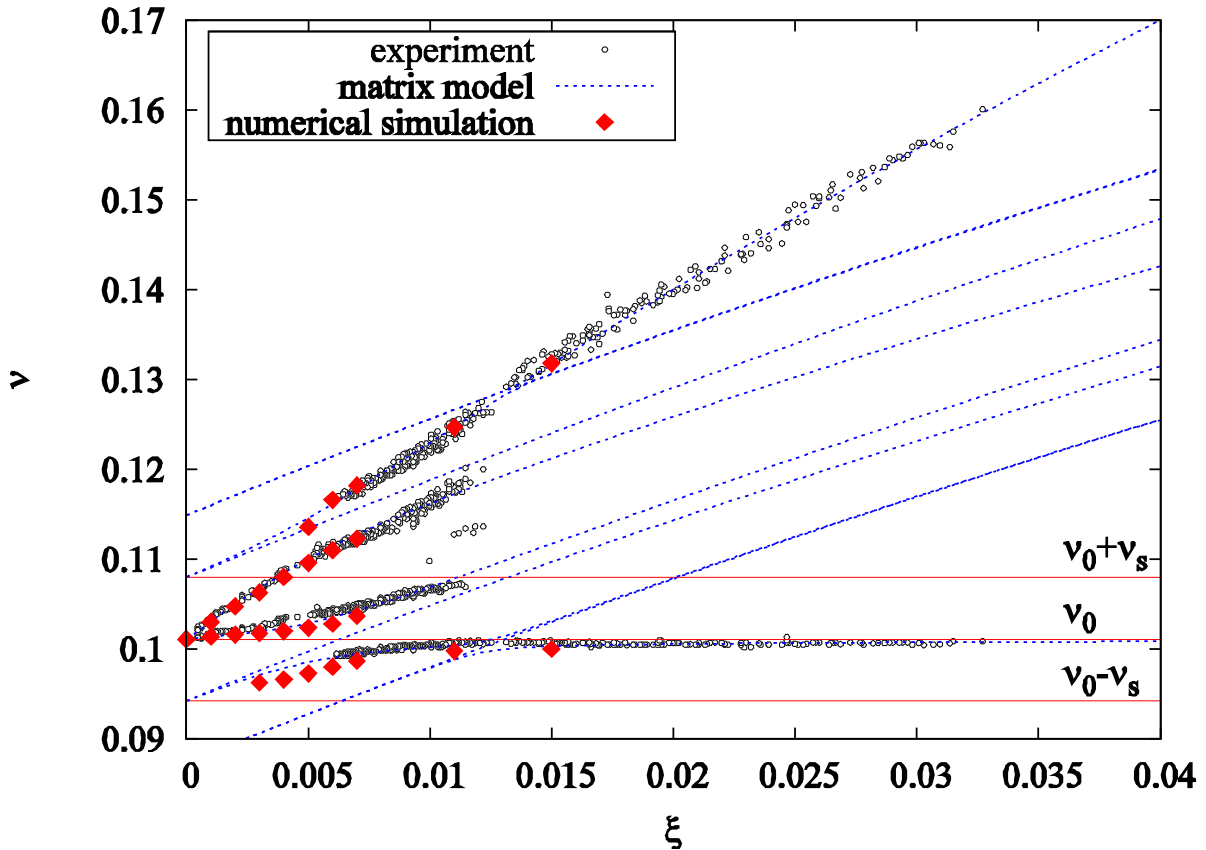


FIG. 2: The diamonds show simulated synchro-betatron modes as a function of beam-beam parameter ξ (diamonds) and of observed modes (points).

predicts instability development at intensities of about 9×10^{12} particles, which is close to where the upper and lower modes meet. We show two sets of curves for two slice and six slice wakefield calculations. The difference between the two slice and six slice simulations is accounted for by the effective slice separation, \hat{z} , that enters Eq. 1. With two slices, the effective \hat{z} is larger than than the six slice effective \hat{z} resulting in a smaller W_0 . With the smaller wake strength, a larger number of protons is necessary to drive the two modes together as is seen in Fig. 4.

The growth rate per turn of dipole motion at the threshold of strong head-tail instability has a parabolic dependence on beam intensity. The wakefield calculation also reproduces this feature as shown in Fig. 5.

Chromaticity interacts with impedance to cause a different head-tail instability. We simulated a range of beam intensities and chromaticity values. The two particle model and

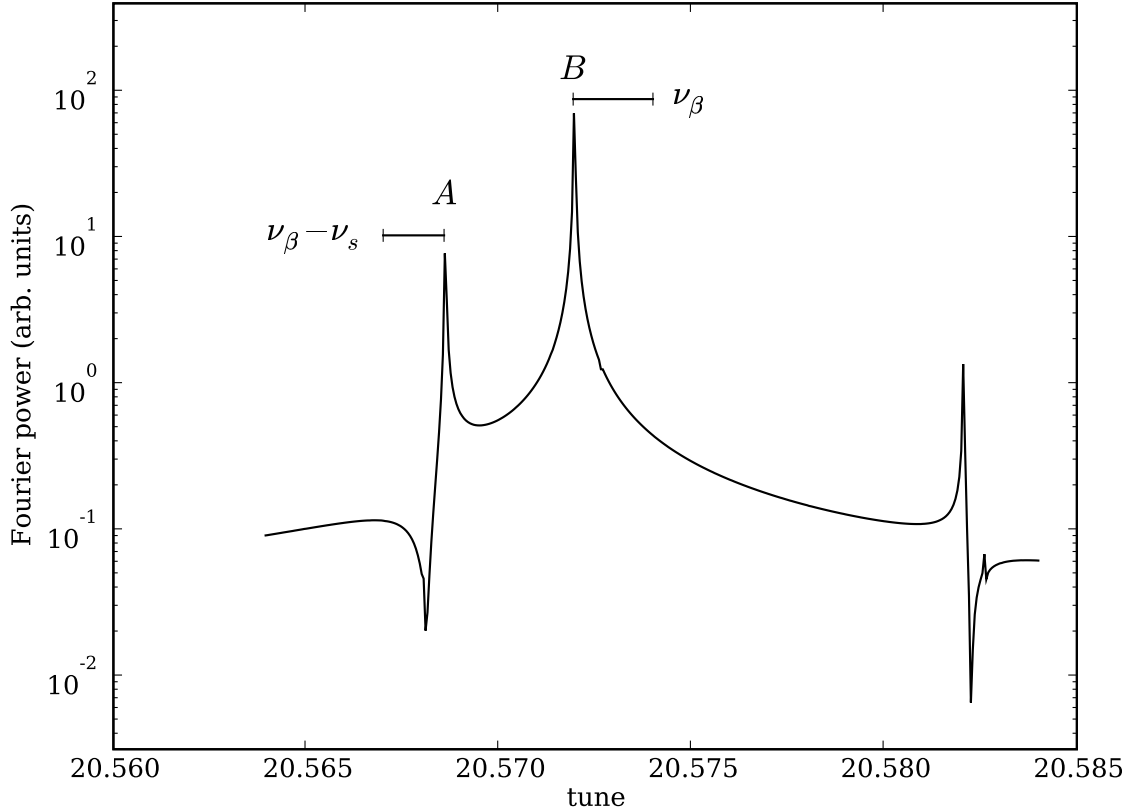


FIG. 3: Simulated spectrum of a two slice bunch in the presence of wakefields and synchrotron motion showing two modes. The bar labeled $\nu_\beta - \nu_s$ shows the upwards shift of the lower synchrotron mode (point *A*.) The bar labeled ν_β shows the downwards shift of the base tune mode (point *B*.)

the more general Vlasov equation calculation [10] indicate that the growth rate scales by the head-tail phase $\chi = 2\pi C\nu_\beta \hat{z}/c\eta$, where η is the slip factor of the machine and \hat{z} is roughly the bunch length. The head-tail phase gives the size of betatron phase variation due to chromatic effects over the length of the bunch.

Some discussion of the meaning of the slip factor in the context of a simulation is necessary. In a real accelerator, the slip factor has an unambiguous meaning: $\eta = (\alpha_C - 1/\gamma^2)$. The momentum compaction parameter α_c is determined by the lattice and γ is the Lorentz factor. We simulate longitudinal motion by applying maps to the particle coordinates z and δ in discrete steps. The simulation parameters specifying longitudinal transport are the

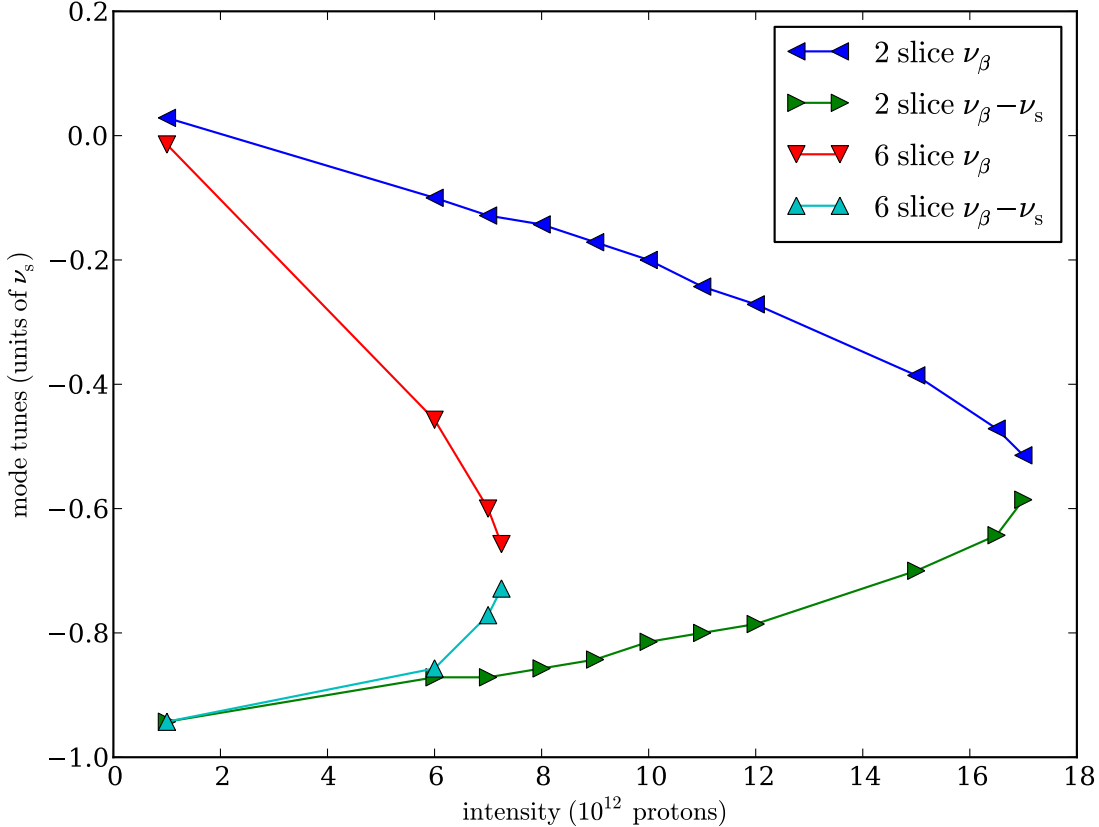


FIG. 4: Evolution of the base tune and lower synchro-betatron mode frequencies as a function of beam intensity showing the two modes approaching a common frequency due to impedance. The y scale is in units of the synchrotron tune. The simulations are shown for a two slice and six slice wakefield calculation.

longitudinal beta function β_z and synchrotron tune ν_s . Note that these parameters do not make reference to path length travelled by a particle. However, path length enters into the impedance calculation because wake forces are proportional to path length. In addition, analytic calculations of the effect of wake forces depend on the evolution of the longitudinal particle position which in turn depend explicitly on the slip factor. For our comparisons with analytic results to be meaningful, we need to use a slip factor that is consistent with the longitudinal maps and the path lengths that enter the wake force calculations. The relationship between the slip factor η and the simulation parameters is $\beta_z = \eta L / 2\pi\nu_s$, where L is the length of the accelerator and $\beta_z = \sigma_z / \sigma_\delta$ is the longitudinal beta function[9, 14] which may

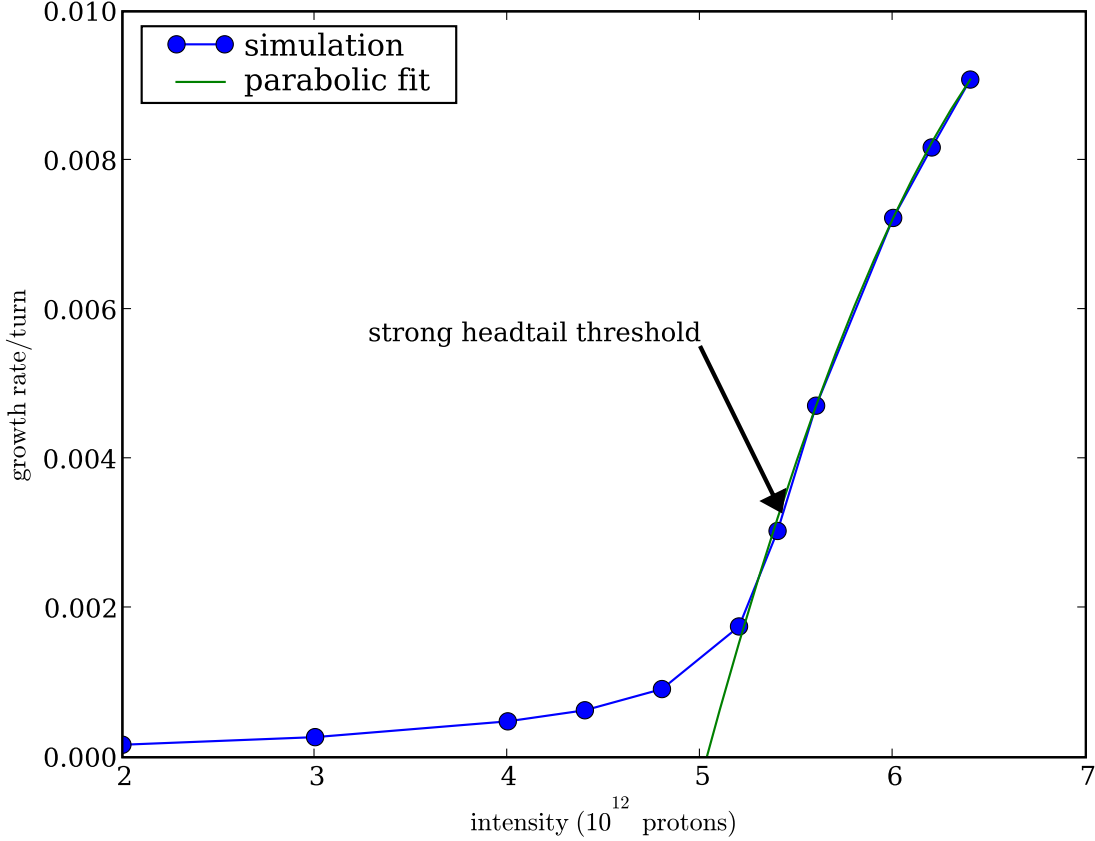


FIG. 5: The growth rate of dipole motion in the simulated accelerator with impedance as a function of beam intensity as the strong head-tail threshold is reached superimposed with a parabolic fit.

be derived by identifying corresponding terms in the solution to the differential equations of longitudinal motion and a one term linear map.

When the growth rate is normalized by $Nr_0W_0/2\pi\beta\gamma\nu_\beta$ which includes the beam intensity and geometric factors, we expect a universal dependence of normalized growth rate versus head-tail phase that begins linearly with head-tail phase[15] and peaks around -1.[18]

Fig. 6 shows the simulated growth rate at three intensities with a range of chromaticities from -0.001 to -0.5 to get head-tail phases in the 0 to -1 range. The normalized curves are nearly identical and peak close to head-tail phase of unity. The deviation from a universal curve is again due to differences between the idealized model and detailed simulation.

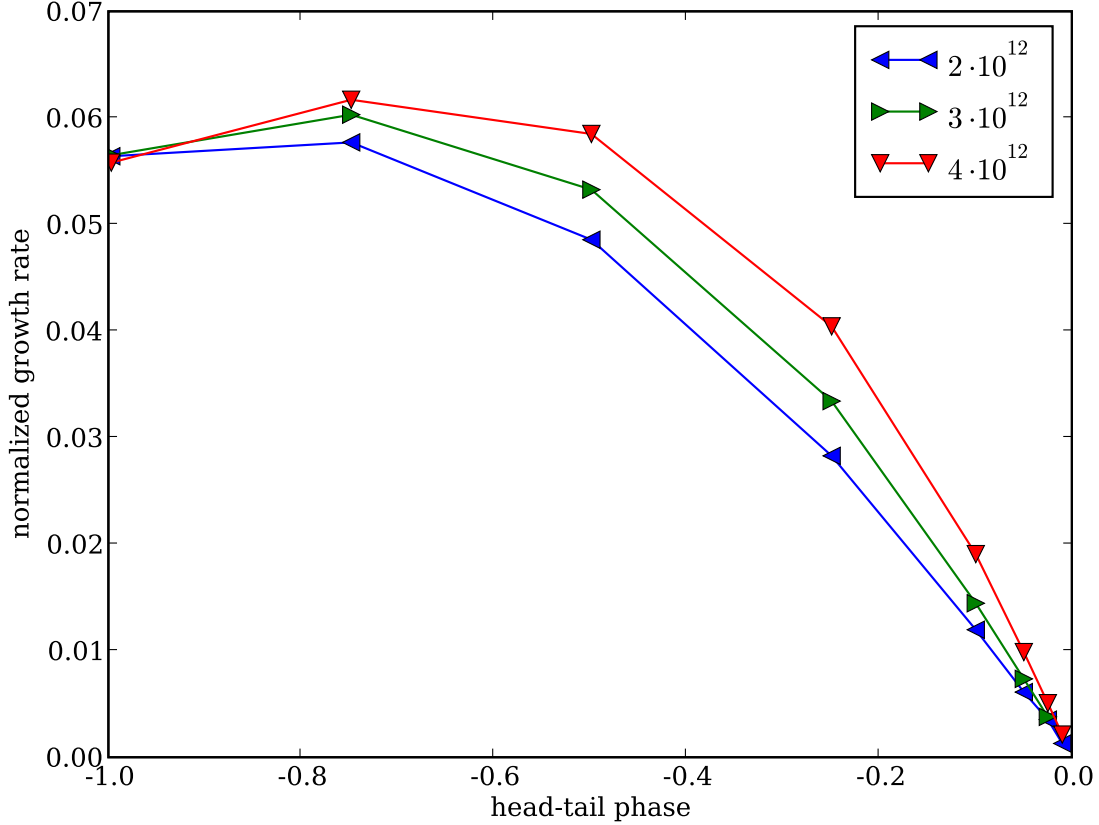


FIG. 6: The normalized growth rate of dipole motion in the simulated accelerator with impedance and chromaticity as a function of head-tail phase χ at three beam intensities demonstrating their linear relationship close to 0 and the near-universal relationship for head-tail phase between -1 and 0 .

V. BUNCH-BY-BUNCH EMITTANCE GROWTH AT THE TEVATRON

The fill pattern of bunches in the Tevatron for protons and antiprotons consists each of three trains of twelve bunches. The bunch train occupies approximately 81.5° separated by a gap of about 38.5° . The bunch train and gap are replicated three times to fill the ring. Bunches collide head-on at the B0 and D0 interaction points but undergo long range (electromagnetic) beam-beam interactions at 136 other locations around the ring. Running the simulation with all 136 long-range IPs turns out to be very slow so we only calculated beam-beam forces at the two main IPs and the long-range IPs immediately upstream and downstream of them. The transverse beta functions at the long-range collision locations

are much larger than the bunch length, so the beam-beam calculation at those locations can be performed using only the 2D solver.

One interesting consequence of the fill pattern and the helical trajectory is that any one of the 12 bunches in a train experiences collisions with the 36 bunches in the other beam at different locations around the ring, and in different transverse positions. This results in a different tune and emittance growth for each bunch of a train, but with the three-fold symmetry for the three trains. This is observed experimentally[16].

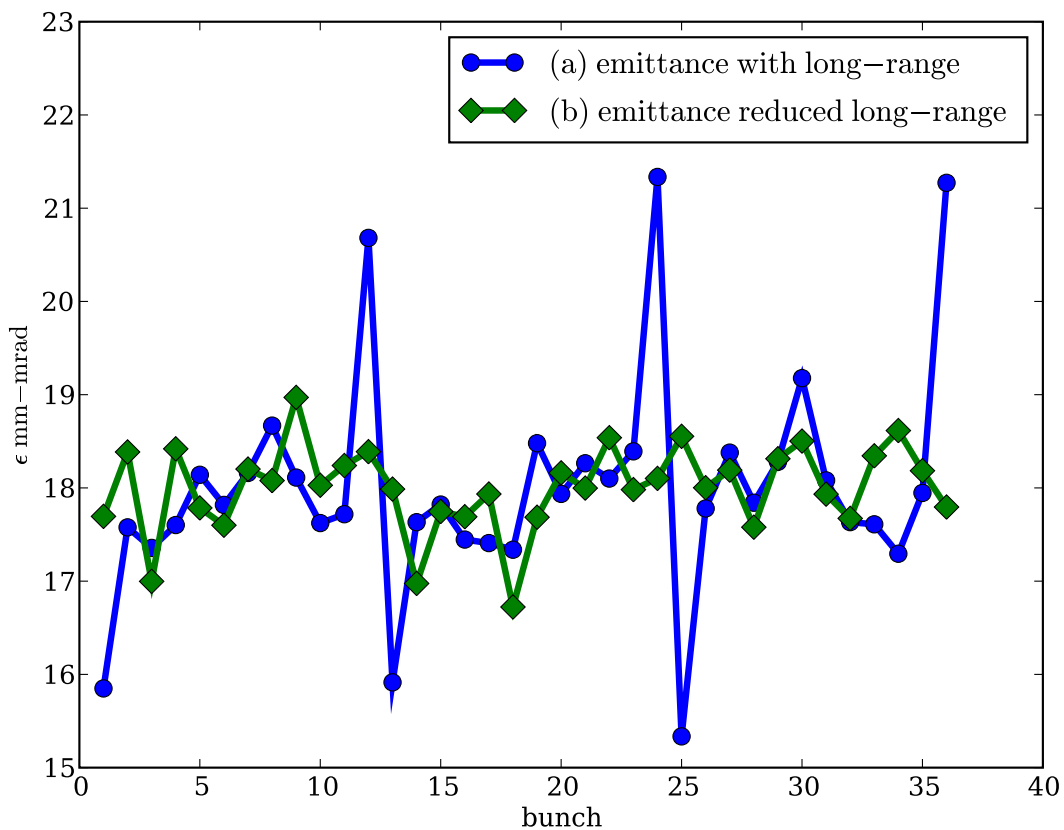


FIG. 7: The emittance of each bunch in a 50000 turn simulation of 36 proton on 36 antiproton bunches in the Tevatron. Curve (a) simulates normal operating conditions with the nominal beam spacing at the long-range IPs. Curve (b) simulates the hypothetical condition with the beam separation at the long-range IPs is 100 times normal, eliminating the the effect of those long-range IPs.

The beam-beam simulation with 36-on-36 bunches shows similar effects. We ran a simu-

lation of 36 proton on 36 antiproton bunches for 50000 turns with the nominal helical orbit. The proton bunches had 8.8×10^{11} particles (roughly four times the usual to enhance the effect) and the proton emittance was the the typical 20π mm-mrad. The antiproton bunch intensity and emittance were both half the corresponding proton bunch parameter. The initial emittance for each proton bunch was the same so changes during the simulation reflect the beam-beam effect.

Curve (a) in Figure 7 shows the emittance for each of the 36 proton bunches in a 36-on-36 simulation after 50000 turns of simulation. The three-fold symmetry is evident. The end bunches of the train are clearly different from the interior bunches. For comparison, Fig. 8 shows the measured emittance taken during accelerator operations. We performed another beam-beam simulation with beam separation at the closest head-on IP expanded 100 times its nominal value resulting in curve (b) of Figure 7 showing a much reduced bunch-to-bunch variation. We conclude that the beam-beam effect at the long-range IPs is the origin of a large part of the bunch variation observed in the running machine.

VI. TEVATRON APPLICATIONS

A. Single bunch features

We looked at the tune spectrum with increasing intensity for p and \bar{p} beams containing one bunch each. As the intensity increases, the beam-beam parameter ξ increases, so we expect increasing separation of the coherent mode tune split. In addition, increasing intensity also causes larger induced wake fields which broaden the mode peaks, especially the π mode, as shown in Fig. 9.

The 4D emittances at higher intensity show significant growth over 20000 turns as shown in Fig. 10. The kurtosis excess of the two beams remains slightly positive for the nominal intensity, but shows a slow increase at higher intensities indicating the the beam core is being concentrated as shown in Fig. 11. Concentration of the bunch core while emittance is growing indicates the development of filamentation and halo.

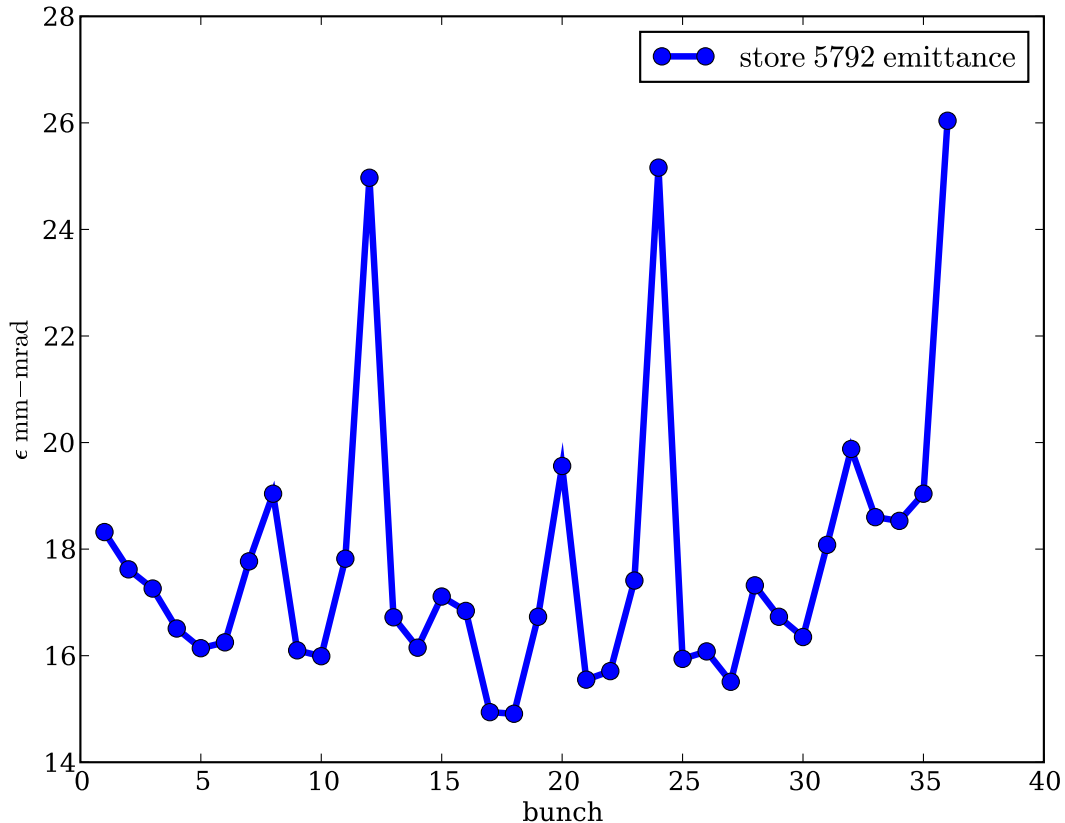


FIG. 8: The measured emittance after 15 minutes of a particular store (#5792) of particles in the Tevatron, showing an emittance growth pattern similar to the simulation results in Figure 7.

B. Simulation of bunch length, synchrotron motion and beam-beam interactions

Synchrotron motion in extended length bunches modifies the effects of the beam-beam interaction by shifting and suppressing the coherent modes. The plots in Fig. 12 show simulated σ and π mode spectra in the vertical plane of one-on-one bunch collisions in a ring with Tevatron-like optics, with both short and long bunches, at three different synchrotron tunes. In this case, “long” bunches are those with bunch lengths comparable to the size of the β function at the interaction point. In this Tevatron simulation, the beam strength is set so that the beam-beam parameter is 0.01, the base tune in the vertical plane is 0.576, β_y is approximately 30 cm. Subplots *a* and *b* of Fig 12 show that with small synchrotron tune both the σ and π mode peaks are evident with short and long bunches. The σ mode peak is at the proper place, with the π mode peak shifted upwards by the expected amount,

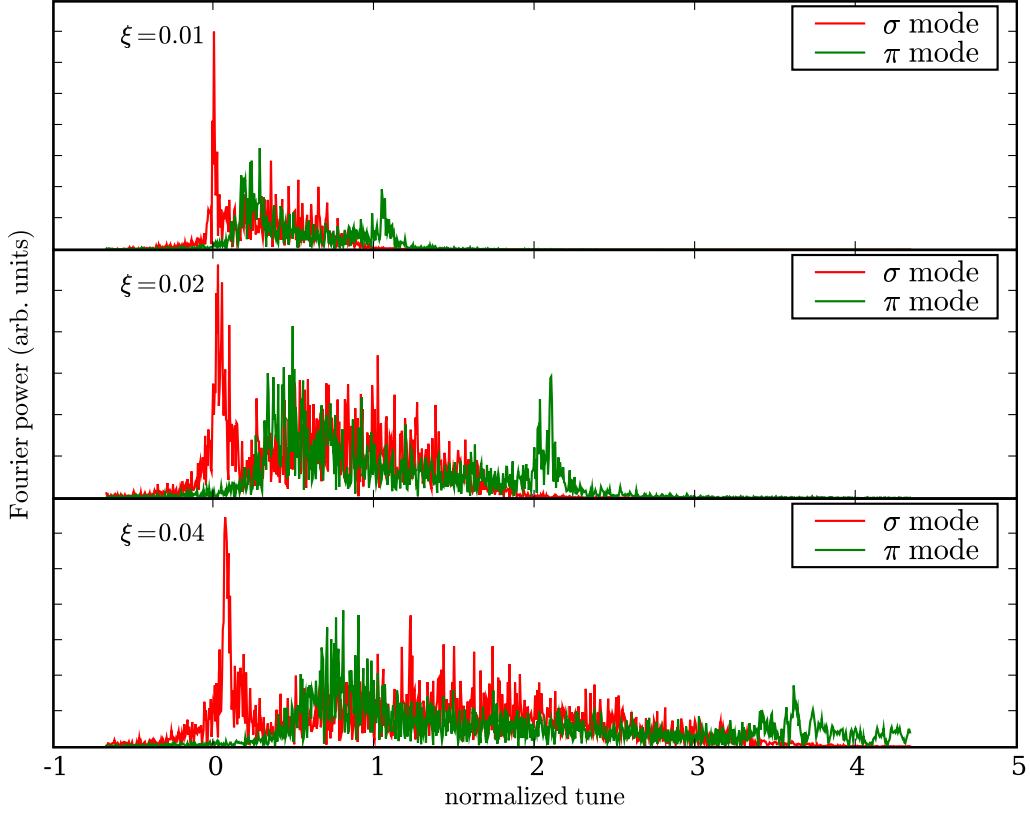


FIG. 9: Dipole mode spectra for two beam σ and π modes at beam intensities of 2.2×10^{11} , 4.4×10^{11} , and 8.8×10^{11} . The corresponding beam-beam parameter is indicated on the plot. The vertical scale is in arbitrary units.

but with longer bunches (subplots *c* and *d*) the incoherent continuum is enhanced and the strength of the coherent peaks is reduced. When the synchrotron tune is the same as or larger than the beam-beam splitting (subplots *e* and *f*) short bunches still exhibit strong coherent modes, but with long bunches the coherent modes are significantly diluted. In the case of long bunches, the σ mode has been shifted upwards to 0.580, and the π mode is not clearly distinguishable from the continuum. At ν_s of 0.01 and 0.02, the synchro-betatron side bands are clearly evident.

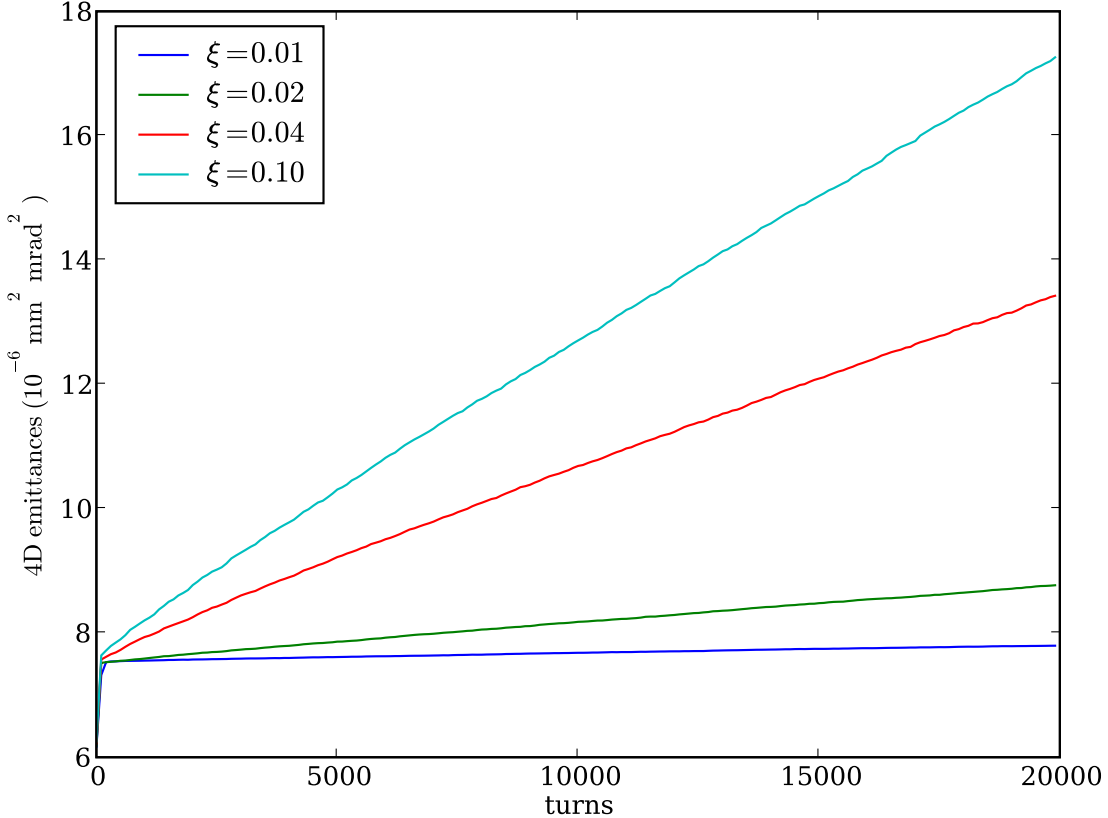


FIG. 10: The evolution of 4D emittances for intensities of (a) 2.2×10^{11} , (b) 4.4×10^{11} , (c) 8.8×10^{11} , and (d) 1.1×10^{12} protons per bunch.

C. Multi-bunch mode studies

When the Tevatron is running in its usual mode, each circulating beam contains 36 bunches. Every bunch in one beam interacts with every bunch in the opposite beam although only two interaction points are useful for high energy physics running. The other 136 interaction points are unwanted and detrimental to beam lifetime and high luminosity. The beam orbit is deflected in a helical shape by electrostatic separators to reduce the impact of these unwanted collisions, so the beams are transversely separated from each other in all but the two high-energy physics interaction points. Because of the helical orbit, each parasitic collision location has its own beam separation and character. A particular bunch experiences collisions at specific interaction points with other bunches each of which has undergone its own collisions. This causes bunch-to-bunch variation in disruption and

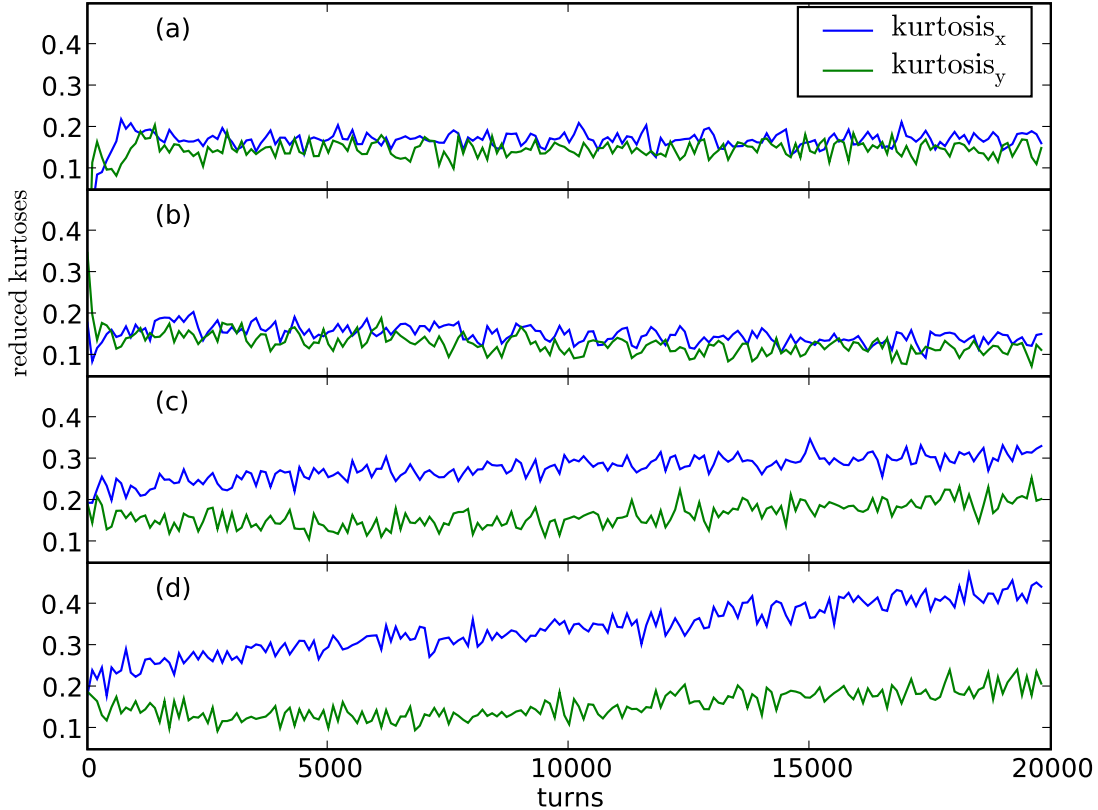


FIG. 11: The evolution of (reduced) kurtosis of the particle distribution for intensities of (a) 2.2×10^{11} , (b) 4.4×10^{11} , (c) 8.8×10^{11} , and (d) 1.1×10^{12} protons per bunch.

emittance growth as will be demonstrated below.

The two head-on interaction points are located 120° around the ring from each other. In these studies, we are only filling the ring with at most six bunches in a beam resulting in ring coverage of about 11° so in effect only one head-on collision location is operating. Because of the beam-beam collisions, each bunch is weakly coupled to every other bunch which gives rise to multi-bunch collective modes.

We began the investigation of these effects with a simulation of beams with two bunches each. The bunches are separated by 21 RF buckets as they are in normal Tevatron operations. Collisions occur at the head-on location and at parasitic locations 10.5 RF buckets distant on either side of the head-on location. To make any excited modes visible, we ran with 2.2×10^{11} particles, which gives a single bunch beam-beam parameter of 0.01.

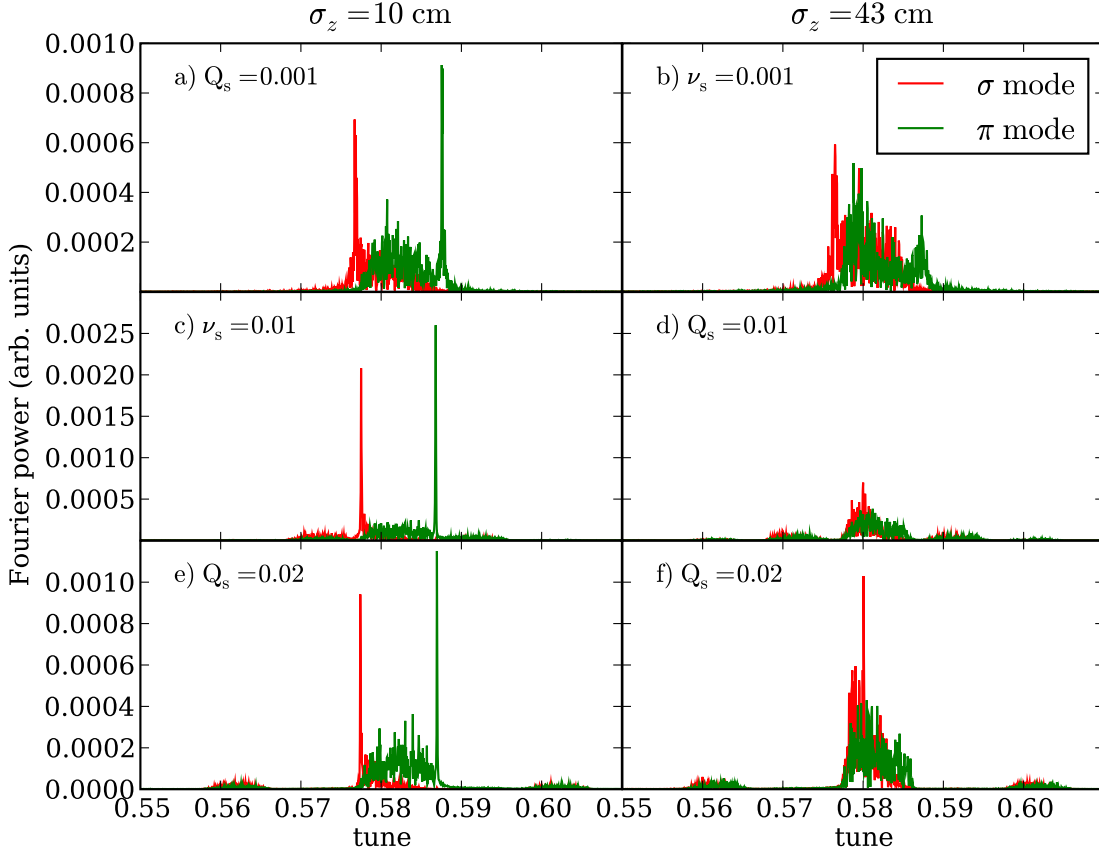


FIG. 12: Simulated one-on-one bunch y plane σ and π mode tune spectra for short bunches (a, c, e) and long bunches (b, d, f), for three different synchrotron tunes, with a Tevatron-like lattice.

There are four bunches in this problem. We label bunch 1 and 3 in beam 1 (proton) and bunch 2 and 4 in beam 2 (antiproton) with mean y positions of the bunches y_1, \dots, y_4 . By diagonalizing the covariance matrix of the turn-by-turn bunch centroid deviations, we determine four modes, shown in Fig. 13. Fig. 13(a) shows the splitting of the σ mode. The coefficients of the two modes indicate that this mode is primarily composed of the sum of corresponding beam bunches (1 with 2, 3 with 4) similar to the σ mode in the one-on-one bunch case. The other two modes in Fig 13(b) have the character and location in tune space of the π mode, from their coefficients and also their reduced strength compared to the σ mode.

With six on six bunches, features emerge that are clearly bunch position specific. Fig. 14(a) shows the turn-by-turn evolution of 4D emittance and (b) y kurtosis for each

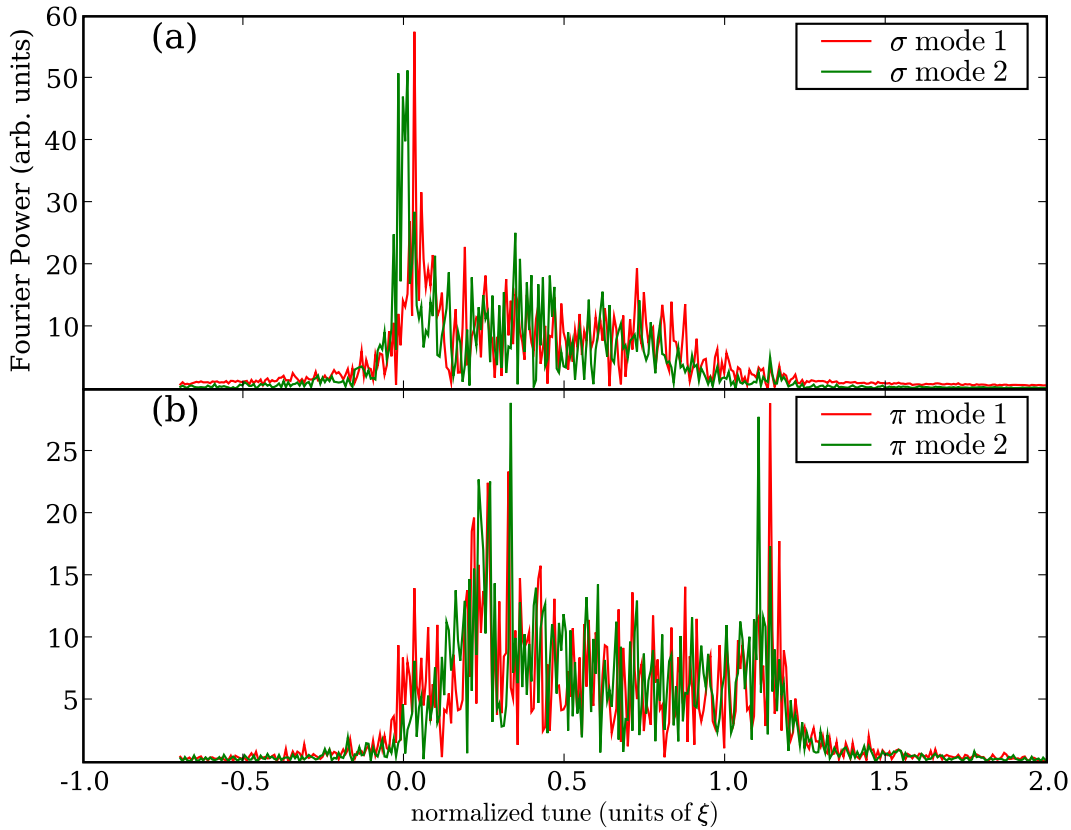


FIG. 13: Mode tune spectrum for a two on two bunch run at 2.2×10^{11} particles/bunch ($\xi = 0.01$). Figure (a) shows the two modes that are most like σ modes. σ mode 1 is $0.53y_1 + 0.53y_2 + 0.59y_3 - 0.31y_4$, σ mode 2 is $0.39y_1 + 0.49y_2 - 0.46y_3 - 0.63y_4$. Figure (b) shows the two π -like modes. π mode 1 is $0.74y_1 - 0.66y_2 - 0.08y_3$, π mode 2 is $0.12y_1 + 0.20y_2 - 0.66y_3 + 0.31y_4$. The absolute scale of the Fourier power is arbitrary, but the relative scales of plots (a) and (b) are the same.

of the six proton bunches. It is striking that bunch 1, the first bunch in the sequence, has a lower emittance growth than all the other bunches. Emittance growth increases faster with increasing bunch number from bunches 2–5, but bunch 6 has a lower emittance growth than even bunch 4. The kurtosis of bunch 1 changes much less than that of any of the other bunches, but bunches 2–5 have very similar evolution, while bunch 6 is markedly closer to bunch 1. One difference between the outside bunches (1 and 6) and the inside bunches (2–5) is that they have only one beam-beam interaction at the parasitic IP closest to the head-on collision, while the inside bunches have one collision before the head-on IP, and one after

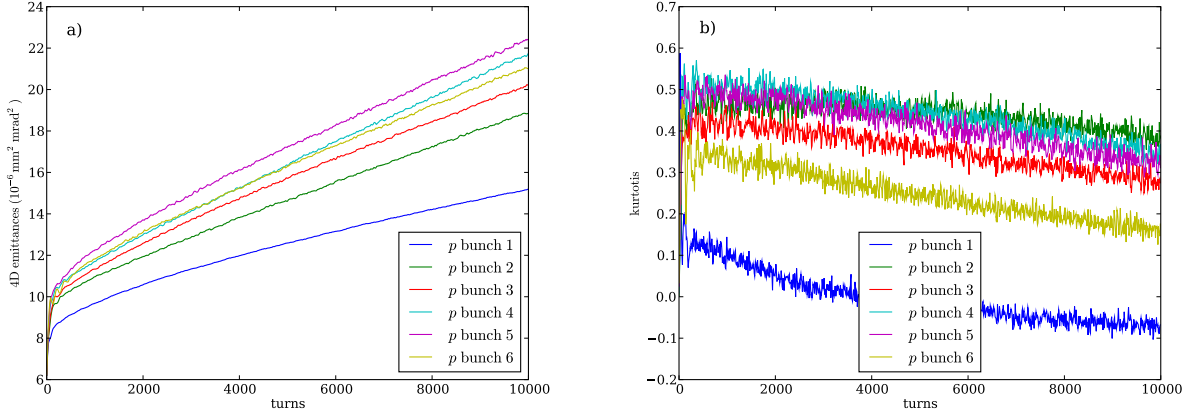


FIG. 14: A six-on-six bunch Tevatron run with 8.8×10^{11} particles/bunch: (a) The turn-by-turn evolution of 4D emittance of each of the six bunches. (b) The turn-by-turn evolution of y kurtosis of the six bunches.

it. The two parasitic collision points closest to the head-on collision point have the smallest separation of any of the parasitics, so interaction there would be expected to disrupt the beam more than interactions at other parasitic locations.

To test this hypothesis, we did two additional runs. In the first, the parasitic IP immediately downstream of the head-on IP was artificially widened so as to have essentially no effect. The effect of this is that the first proton bunch will not have any beam-beam collisions at an IP close to the head-on IP, while all the other bunches will have one collision at a near-head-on IP. The corresponding plots of emittance and kurtosis are shown in Fig. 15. The kurtosis data shows that bunches 2–5 which all suffer one beam-beam collision at a close parasitic IP are all together while bunch 1 which does not have a close IP collision is separated from the others.

Emittance and kurtosis growth in runs where both upstream and downstream closest parasitic IPs were artificially widened is shown in Fig. 16. In this configuration no bunch suffers a strong beam-beam collision at a parasitic IP close to the head-on location so the kurtosis of all the bunches evolves similarly.

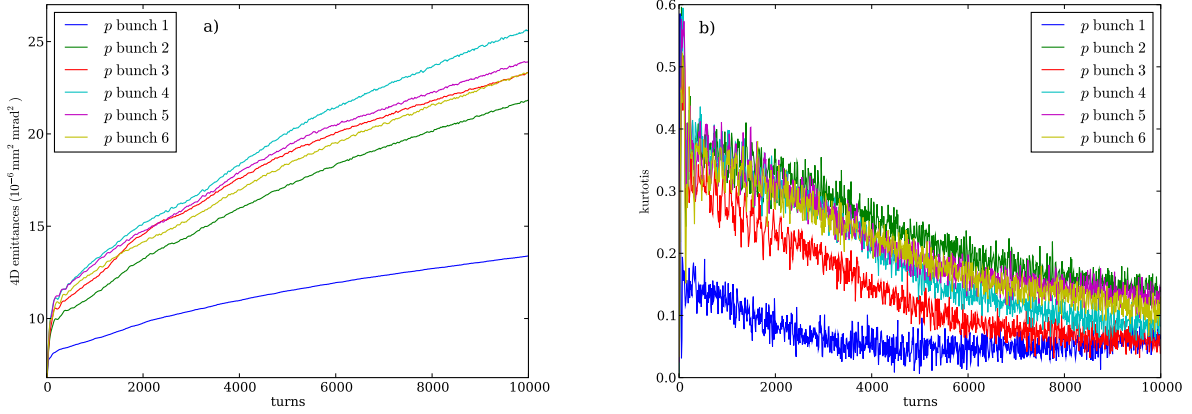


FIG. 15: In a six-on-six bunch Tevatron run with 8.8×10^{11} particles/bunch, with the first parasitic IP downstream of the head-on location artificially widened: (a) The 4D emittance of each of the six bunches as a function of turn. (b) the y kurtosis of the six bunches as a function of turn.

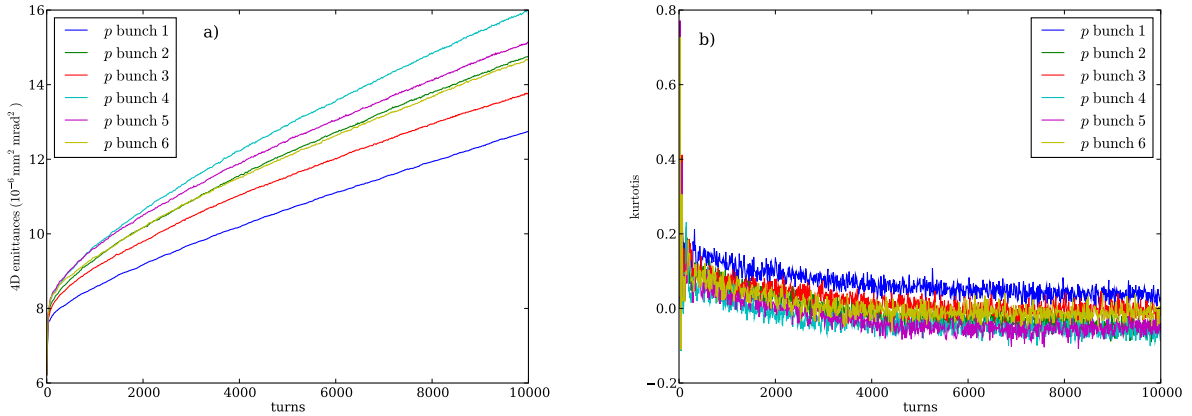


FIG. 16: In a six-on-six bunch Tevatron run with 8.8×10^{11} particles/bunch, with the both nearest upstream and downstream parasitic IP artificially widened: (a) The 4D emittance of each of the six bunches as a function of turn. (b) the y kurtosis of the six bunches as a function of turn.

VII. LOWER CHROMATICITY THRESHOLD

During the Tevatron operation in 2009 the limit for increasing the initial luminosity was determined by particle losses in the so-called squeeze phase [17]. At this stage the beams are separated in the main interaction points (not colliding head-on), and the machine optics is gradually changed to decrease the beta-function at these locations from 1.5 m to 0.28 m.

With proton bunch intensities currently approaching 3.2×10^{11} particles, the chromatic-

ity of the Tevatron has to be managed carefully to avoid the development of a head-tail instability. It was determined experimentally that after the head-on collisions are initiated, the Landau damping introduced by beam-beam interaction is strong enough to maintain beam stability at chromaticity of +2 units. At the earlier stages of the collider cycle, when beam-beam effects are limited to long-range interactions the chromaticity was kept as high as 15 units since the concern was that the Landau damping is insufficient to suppress the instability. At the same time, high chromaticity causes particle losses which are often large enough to quench the superconducting magnets, and hence it is desirable to keep it at a reasonable minimum.

TABLE I: Beam parameters for Tevatron simulation

Parameter	value
beam energy	980 GeV
p particles/bunch	3.0×10^{11}
\bar{p} particles/bunch	0.9×10^{11}
p tune (Q_x, Q_y)	(20.585,20.587)
p (normalized) emittance	20π mm-mrad
\bar{p} tune (Q_x, Q_y)	(20.577,20.570)
\bar{p} (normalized) emittance	6π mm-mrad
synchrotron tune Q_s	0.0007
slip factor	0.002483
bunch length (rms)	43 cm
$\delta p/P$ momentum spread	1.2×10^{-4}
effective pipe radius	3 cm

Our multi-physics simulation was used to determine the safe lower limit for chromaticity. The simulations were performed with starting beam parameters listed in Table I. With chromaticity set to -2 units, and no beam-beam effect, the beams are clearly unstable as seen in Fig. 17. With beams separated, turning on the beam-beam effect prevents rapid oscillation growth during the simulation as shown in Fig. 18. The bursts of increased amplitude is sometimes indicative of the onset of instability, but it is not obvious within the limited duration of this run. The RMS size of the beam also does not exhibit any obvious unstable

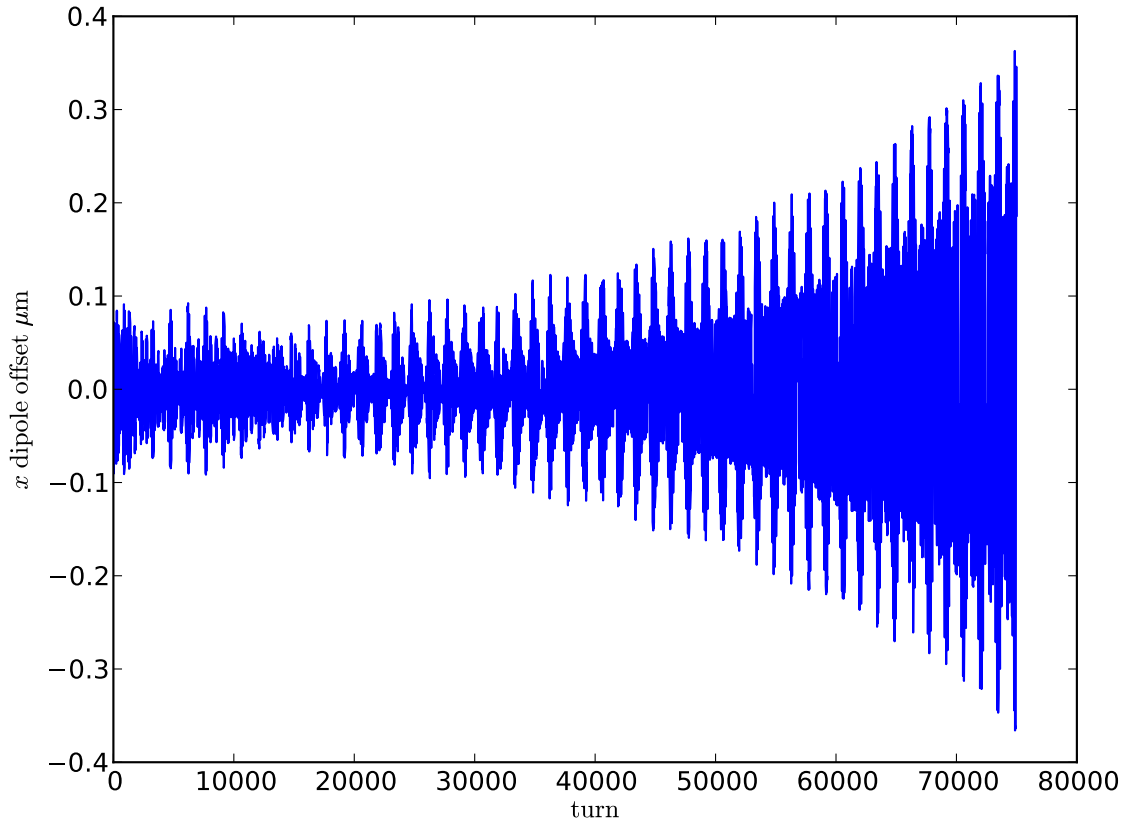


FIG. 17: The x dipole moment in a simulation with $C = -2$ and no beam-beam effect showing the development of instability.

tendencies as shown in Fig. 19.

Based on these findings the chromaticity in the squeeze was lowered by a factor of two, and presently is kept at 8-9 units. This resulted in a significant decrease of the observed particle loss rates (see, *e.g.*, Fig. 5 in [17]).

VIII. SUMMARY

The key features of the developed simulation include fully three-dimensional strong-strong multi-bunch beam-beam interactions with multiple interaction points, transverse resistive wall impedance, and chromaticity. We have validated the correctness of modules that simulate individual processes using available experimental data and analytical models.

Integrated beam-beam simulations have reproduced features of the observed bunch-to-

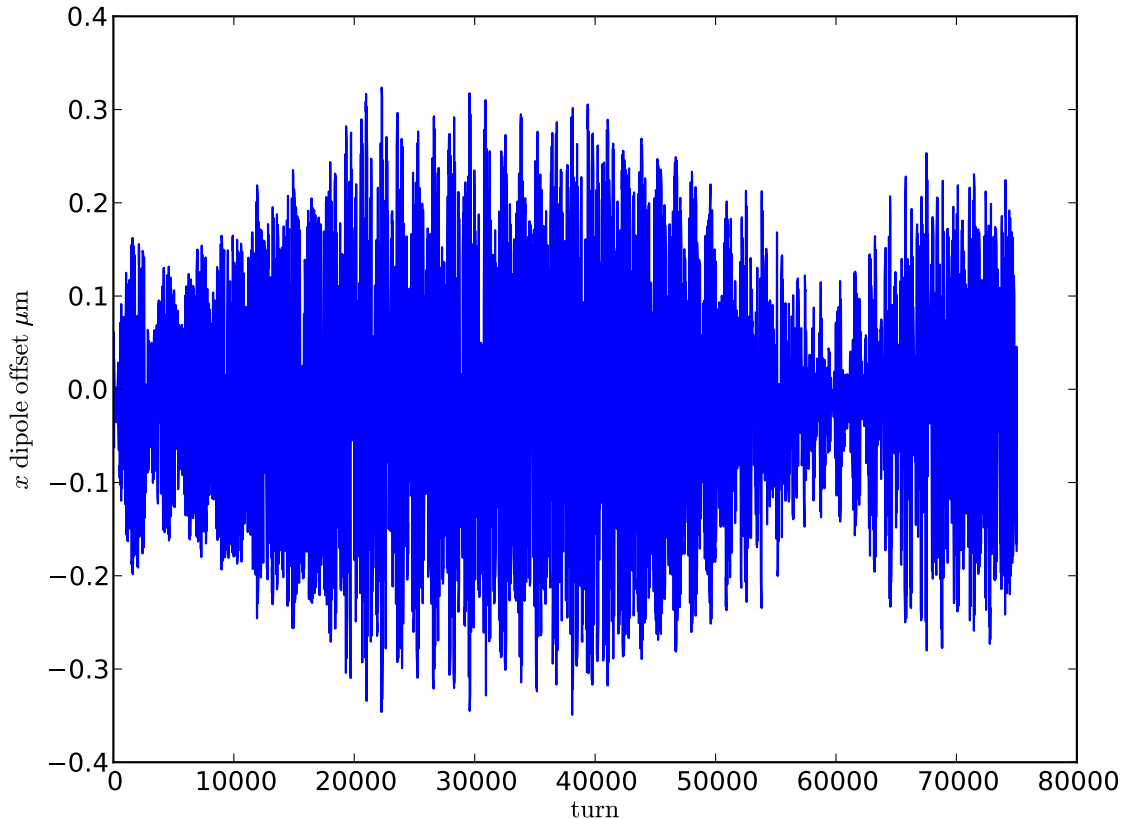


FIG. 18: The x dipole moment of a representative bunch in a 36-on-36 simulation with $C = -2$ with beam-beam effects and beams separated showing no obvious instability within the limits of the simulation.

bunch dynamics at the Tevatron.

The new program is a valuable tool for evaluation of the interplay between the beam-beam effects and transverse collective instabilities. Simulations have been successfully used to support the change of chromaticity at the Tevatron, demonstrating that even the reduced beam-beam effect from long-range collisions may provide enough Landau damping to prevent the development of head-tail instability.

Acknowledgments

We thank J. Qiang and R. Ryne of LBNL for the use of and assistance with the Beam-Beam3d program. We are indebted to V. Lebedev and Yu. Alexahin for useful discus-

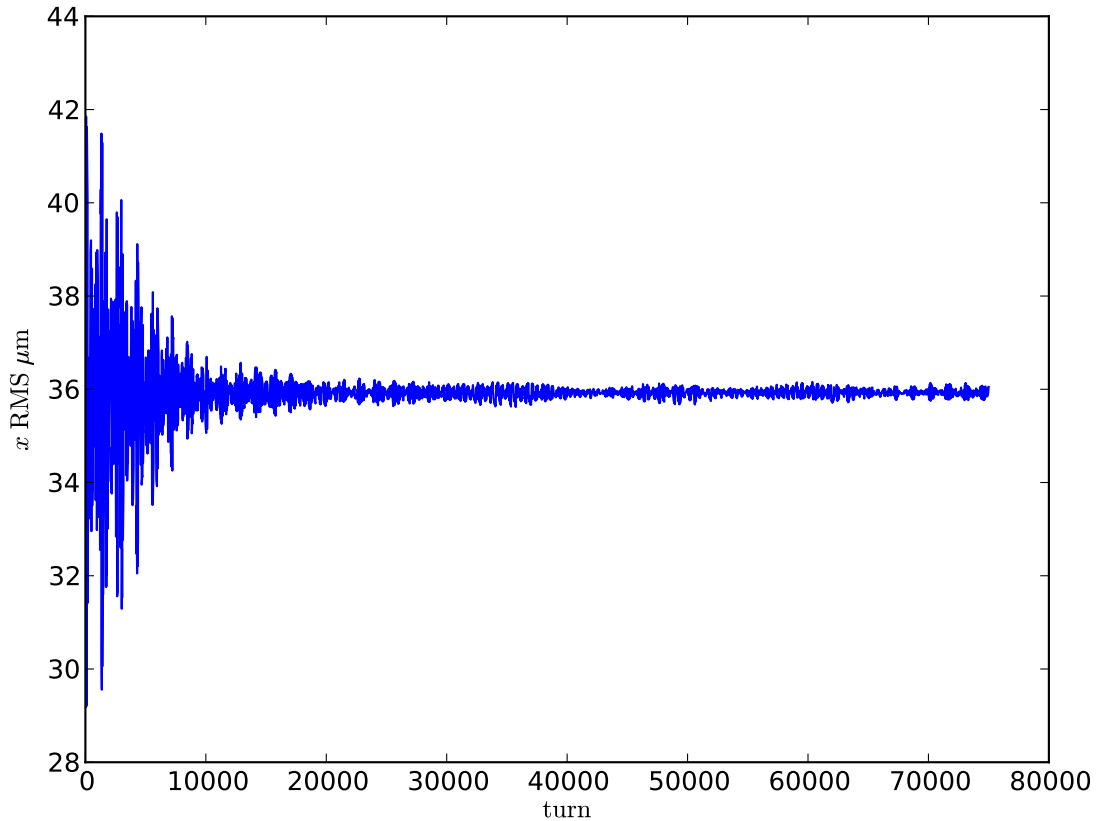


FIG. 19: The x dipole moment of a representative bunch in a 36-on-36 simulation with $C = -2$ with beam-beam effects and beams separated showing no obvious instability within the limits of the simulation.

sions. This work was supported by the United States Department of Energy under contract DE-AC02-07CH11359 and the ComPASS project funded through the Scientific Discovery through Advanced Computing program in the DOE Office of High Energy Physics. This research used resources of the National Energy Research Scientific Computing Center, which is supported by the Office of Science of the U.S. Department of Energy under Contract No. DE-AC02-05CH11231. This research used resources of the Argonne Leadership Computing Facility at Argonne National Laboratory, which is supported by the Office of Science of the

- [1] Run II handbook, <http://www-bd.fnal.gov/runII>
- [2] A. Valishev *et al.*, “Observations and Modeling of Beam-Beam Effects at the Tevatron Collider”, PAC2007, Albuquerque, NM, 2007
- [3] M. Xiao *et al.*, “Tevatron Beam-Beam Simulation at Injection Energy”, PAC2003, Portland, OR, 2003
- [4] Y. Alexahin, “On the Landau Damping and Decoherence of Transverse Dipole Oscillations in Colliding Beams”, *Part. Acc.* **59**, 43 (1996)
- [5] E.A. Perevedentsev and A.A. Valishev, “Simulation of Head-Tail Instability of Colliding Bunches”, *Phys. Rev. ST Accel. Beams* **4**, 024403, (2001)
- [6] J. Qiang, M.A. Furman, R.D. Ryne, *J.Comp.Phys.*, 198 (2004), pp. 278–294, J. Qiang, M.A. Furman, R.D. Ryne, *Phys. Rev. ST Accel. Beams*, 104402 (2002).
- [7] V. Lebedev, <http://www-bdnew.fnal.gov/pbar/organizationalchart/lebedev/OptiM/optim.htm>
- [8] A. Valishev *et al.*, “Progress with Collision Optics of the Fermilab Tevatron Collider”, EPAC06, Edinburgh, Scotland, 2006
- [9] A. Chao, *Physics of Collective Beam Instabilities in High Energy Accelerators.*, p. 9, John Wiley and Sons, Inc., (1993)
- [10] A. Chao, *Physics of Collective Beam Instabilities in High Energy Accelerators.*, pp. 56–60, 178–187, 333–360 John Wiley and Sons, Inc., (1993)
- [11] I.N. Nesterenko, E.A. Perevedentsev, A.A. Valishev, *Phys.Rev.E*, 65, 056502 (2002)
- [12] A. Piwinski, *IEEE Trans. Nucl. Sci.* **NS-26** (3), 4268 (1979).
- [13] K. Yokoya, *Phys. Rev. ST-AB* **3**, 124401 (2000).
- [14] D.A. Edwards and M.J. Syphers, *An Introduction to the Physics of High Energy Accelerators*, pp. 30–46, John Wiley and Sons Inc., 1993.
- [15] A. Chao, *Physics of Collective Beam Instabilities in High Energy Accelerators.*, p. 351, John Wiley and Sons, Inc., (1993).
- [16] V. Shiltsev, *et al.*, “Beam-Beam Effects in the Tevatron,” *PRSTAB*, **8**, 101001 (2005).
- [17] A. Valishev *et al.*, “Recent Tevatron Operational Experience”, PAC2009, Vancouver, BC, 2009

[18] The simulated machine is above transition (η is positive.) The head-tail instability develops when chromaticity is negative, thus the head-tail phase is negative.